Journal of The Electrochemical Society, **165** (11) F986-F993 (2018)
0013-4651/2018/165(11)/F986/8/$37.00 © The Electrochemical Society

Investigating the In-/Through-Plane Effective Diffusivities of Dry and Partially-Saturated Gas Diffusion Layers

Zhiqiang Niu,[1,2] Jingtian Wu,[2] Yun Wang,[2,*,z] and Kui Jiao[1,z]

[1] *State Key Laboratory of Engines, Tianjin University, Tianjin 300350, People's Republic of China*
[2] *Renewable Energy Resources Lab (RERL) and National Fuel Cell Research Center, Department of Mechanical and Aerospace Engineering, University of California, Irvine, California 92697-3975, USA*

In this study, the effective oxygen diffusivity in the dry or partially-saturated gas diffusion layer (GDL) is numerically investigated by an oxygen diffusion model in GDLs reconstructed by a stochastic method. The predicted effective diffusivity in dry GDLs is compared with various diffusivity models from literatures. Reasonable agreements with other models were obtained. The effect of the PTFE loading in the dry Toray carbon paper is also investigated and compared with recent experimental data. It is found that the effective diffusivity becomes lower under higher PTFE loading due to the decreased pore volume, as expected. The relative effective oxygen diffusivity in partially-saturated GDLs is calculated using the two-phase volume of fluid (VOF) model and an oxygen diffusion model. The effects of different local water profiles and porosity distribution on the effective oxygen diffusivity in both the through-plane (TP) and in-plane (IP) directions are investigated and compared with a lattice Boltzmann model and experimental data. The present results are in good agreement with other studies. It is found that local water profile has significant impacts on the effective diffusivity in partially-saturated GDLs and the diffusivity in the TP direction is more sensitive to the water distribution than the IP direction.
 [DOI: 10.1149/2.1191811jes]

Manuscript submitted July 23, 2018; revised manuscript received August 24, 2018. Published September 5, 2018.

Proton exchange membrane (PEM) fuel cells have shown great potential as alternative power sources for the electric vehicles due to their outstanding merits such as high efficiency, negligible emissions and high power density. For high-performance PEM fuel cells, one of the major challenges is flooding of the gas diffusion layer (GDL) due to water production by the catalyst layer (CL), which hampers the oxygen transport to the CL sites, thereby reducing fuel cell performance.[1,2] Thus, comprehensive understanding of effective oxygen transport in the partially-saturated GDL is critical to optimize the GDL structure design and enhance fuel cell performance.[3,4]

GDLs are generally fibrous porous media, composing of randomly oriented carbon fibers, as shown in Fig. 1. GDLs fulfill several important functions in the operation of PEM fuel cells, e.g. providing the transport pathways for reactant oxygen, product water, heat, and electrons. Liquid water may appear in GDLs or at the GDL surface, as shown in Fig. 1, which hampers gas transport by increasing the transport path. In partially-saturated GDLs, the effective diffusivity can be modeled with respect to the porosity ε and water saturation s as two independent functions,

$$\frac{D_{eff}^{wet}}{D_{bulk}} = \frac{\varepsilon}{\tau} = \frac{D_{eff}^{dry}}{D_{bulk}} \frac{D_{eff}^{wet}}{D_{eff}^{dry}} = f(\varepsilon)\, g(s) \qquad [1]$$

where D_{eff}^{wet} ($m^2\ s^{-1}$) and D_{eff}^{dry} ($m^2\ s^{-1}$) the effective diffusivity in the dry and partially-saturated GDLs, respectively. D_{bulk} ($m^2\ s^{-1}$) the bulk diffusivity. τ the tortuosity. $f(\varepsilon)$ and $g(s)$ are two normalized functions which are scaled from 0 to 1, where $f(\varepsilon)$ describes the relative effective diffusivity in the dry GDL (i.e. $g(s) = 1$), and $g(s)$ describes that in the partially-saturated (or wet) GDL. In PEM fuel cells, GDLs can be subjected to both dry and wet operation, and the anode GDL may be flooded by liquid water as well.[5]

For dry GDLs, many experimental measurements[6–8] and numerical studies[9–15] suggested the relative effective diffusivity function $f(\varepsilon)$ is strongly dependent on the porosity ε, as summarized in Table I. However, these models are mostly based on the effective medium theory (M-1, M-4), pore network model (M-3, M-5), random fiber theory (M-2) or random fiber theory (M-2) and neglect several important features in GDLs such as Polytetrafluoroethylene (PTFE) loading, compression and so on. Therefore, the detailed GDL morphology should be counted in order to obtain accurate effective oxygen diffusivity.

In recent, several studies investigated the transport properties in dry GDLs digitally reconstructed by stochastic methods or X-ray tomography.[16–20] Backer et al.[16] reconstructed a dry Toray-060 carbon paper using both the stochastic method and X-ray tomographic microscopy to numerically investigate the diffusivity, permeability and electric conductivity of the GDL under different compressions. They conducted experiment to validate their numerical results. Wang et al.[17] numerically solved transport equations in a stochastic model reconstructed GDL, and found that the tortuosity of the pore and fiber networks are about 1.2 and 13, respectively. Espinoza et al.[18] adopted the lattice Boltzmann (LB) method to study the diffusivity in the through-plane (TP) direction of a dry GDL and compared with various correlations. They indicated that the Tomadakis and Sotirchos's model (M-2) shows better prediction than the Bruggeman's model (M-1). Though many studies have been attempted to investigate the diffusivity in GDLs, few have presented a comprehensive comparison with experimental data including the impacts of both PTFE loading in dry samples and liquid water saturation.

For partially-saturated GDLs, few experiments[7,21–26] have been attempted to measure the relative effective diffusivity $g(s)$ because of the difficulty in obtaining the mass flux and concentration between the two sides of a GDL with a thickness ranging from 100 μm to 400 μm and the water saturation in GDLs. Hwang and Weber etal.[7] used an ex-situ electrochemical limiting-current method to measure the effective diffusivity of various unsaturated and partially-saturated GDLs of different PTFE loadings. They found that the effective diffusivity is a function of the water saturation $g(s) = (1\text{-}s)^3$ in the through-plane (TP) direction, with no significant variation among the selected fiber structures. Tranter et al.[25] developed a new method to measure the in-plane (IP) diffusivity of partially-saturated GDLs. They found the relative IP diffusivity follow a power-law correlation, consistent with previous modeling results. Wang et al.[26] utilized an oxygen sensor based on a galvanic cell to measure the effective oxygen diffusivity in two typical GDLs of Toray-H-120 carbon paper and carbon cloth under both dry and partially-saturated conditions. They found that the effective oxygen diffusivity strongly depends on the pore size distribution and water saturation in GDLs.

As alternative, numerical modeling is an effective method to investigate the effective diffusivity in partially-saturated GDLs. Several approaches have been attempted using pore-morphology (PM) model,[16,27–29] LB model,[24,30–33] pore network (PN) model[34,35] and finite volume method (FVM).[17,19,36] Zamel et al.[27] used a PM model to investigate the effects of liquid water presence on the transport properties of the carbon paper GDL and examine various laws to estimate the transport properties in the presence of liquid water. They found that the effect of liquid water is more significant in the TP direction than in the IP one. García-Salaberri et al.[31] performed LB simulations

*Electrochemical Society Member.
[z]E-mail: yunw@uci.edu; kjiao@tju.edu.cn

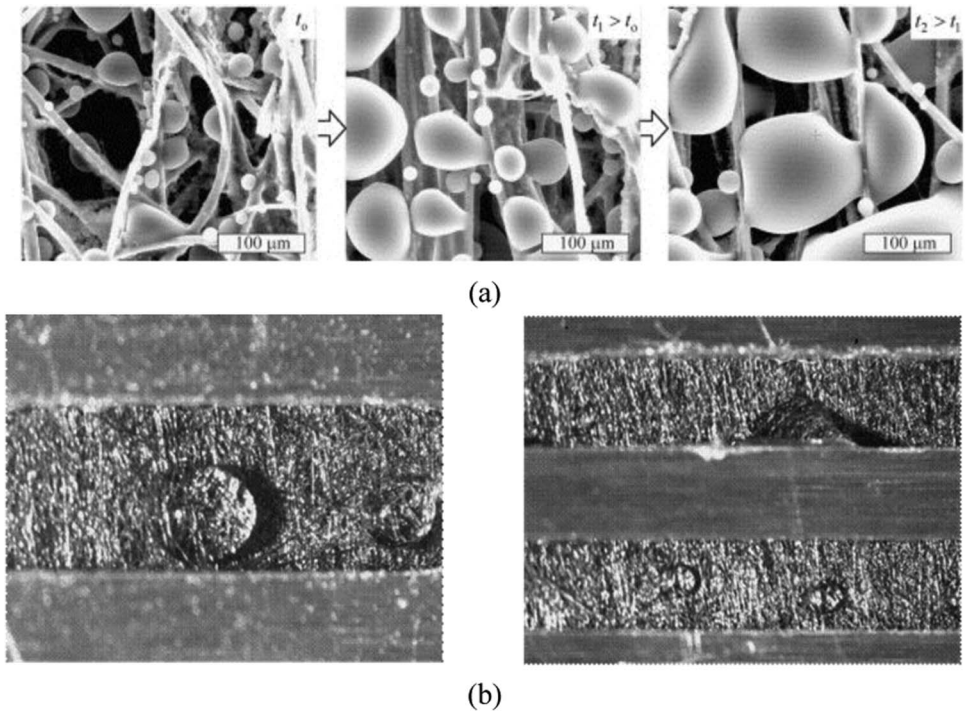

Figure 1. (a) Liquid water formation (vapor condensation) in the GDL imaged by environmental scanning electron microscope technique[2] and (b) break-through water at the GDL surface imaged by optical microscopy.[4]

on the X-ray tomographic reconstructions of invading liquid water to determine the effective diffusivity for carbon-fiber GDLs. Their results are in good agreement with previous experimental data. They found that the liquid's impact on gas transport is highly dependent on the local saturation in GDLs. Wu et al.[35] adopted a PN model to investigate the effect of the GDL structural parameters on the effective oxygen diffusivity under both dry and partially-saturated conditions. They proposed two new correlations to determine the oxygen effective diffusivity for the Toray carbon paper GDLs. Moosavi et al.[36] utilized a FVM model to investigate the transport characteristics based on a tomography reconstructed GDL. Their results were compared with reported experimental data and semi-empirical correlations.

Through several numerical studies have been performed to study the effective oxygen diffusivity in dry and partially-saturated GDLs, few investigated the impacts of local porosity distribution and water saturation distribution in the TP direction. In addition, validation against experimental data is largely absent.[31–33,36] One major reason is that those detailed local porosity and water saturation distribution were only available recently when high-resolution X-ray computed tomography (XCT) imaging technique were introduced to GDL studies. In this study, a three-dimensional (3D) two-phase volume of fluid (VOF) model,[37] along with a stochastic model of GDL microstructures reconstruction, was applied to obtain the water saturation distribution inside the Toray carbon papers (TGP-H-120 and TGP-H-060). An oxygen diffusion model was developed to simulate oxygen diffusion in both dry and partially-saturated GDLs. The simulated relative effective oxygen diffusivity $f(\varepsilon)$ in the dry and partially-saturated GDLs were compared with various models (listed in Table I), LB results,[31] PM model results[27,29] as well as experiment data.[7,24] This study is one of the first approaches that combine the VOF method and oxygen diffusion model to investigate the effective oxygen diffusivity $g(s)$ in partially-saturated GDLs.

Model Formulation

In the present model, several assumptions are made as follows:

1) The flows in the GDLs are uncompressible and laminar flow.
2) The physical properties of air, water and oxygen are constant.
3) The contact angle of the fiber surface is constant.
4) PTFE in GDLs is randomly distributed.
5) The phase change between liquid water and vapor is ignored.

VOF model.—In the two-phase VOF model, the liquid water phase fraction γ is introduced as a main variable to be solved. The cells fully occupied by liquid water are marked as $\gamma = 1$, whereas cells fully occupied by air are marked as $\gamma = 0$. The cells with phase fraction between 0 and 1 consist of air-water interface. The volume averaged

Table I. Various models of the effective diffusivity in GDLs.

$f(\varepsilon)$	$g(s)$	Ref.	Label
$\varepsilon_{avg}{}^{1.5}$	1	Bruggman et al.[9]	M-1
$\varepsilon_{avg}(\frac{\varepsilon_{avg}-0.037}{1-0.037})^{0.661}$	1	Tomadakis & Sotirchos[10]	M-2
$\varepsilon_{avg}(\frac{\varepsilon_{avg}-0.11}{1-0.11})^{0.785}$	$(1-s_{avg})^{\beta}$, $\beta = 2.0$	Nam and Kaviany[11]	M-3
$1-\frac{3(1-\varepsilon_{avg})}{3-\varepsilon_{avg}}$	1	Das et al.[12]	M-4
$1-(1-\varepsilon_{avg})^{0.46}$	1	Mezedur et al.[13]	M-5
$\varepsilon_{avg}{}^{3.8}$	1	Martínez et al.[14]	M-6

density and dynamic viscosity for air-water mixture, ρ (kg m^{-3}) and μ (kg m^{-1} s^{-1}), are calculated as follows:

$$\rho = \rho_l \gamma + \rho_g (1-\gamma) \quad [2]$$

$$\mu = \mu_l \gamma + \mu_g (1-\gamma) \quad [3]$$

where subscripts l and g denote the liquid phase and gas phase respectively.

The governing equations for the two-phase VOF model in this study are listed as follows:[37,38,41]

Continuity equation:

$$\nabla \cdot \vec{U} = 0 \quad [4]$$

Phase conservation equation:

$$\frac{\partial \gamma}{\partial t} + \nabla \cdot \left(\vec{U}\gamma\right) + \nabla \cdot \left[\vec{U}_r \gamma (1-\gamma)\right] = 0 \quad [5]$$

Momentum equation:

$$\frac{\partial(\rho\vec{U})}{\partial t} + \nabla \cdot \left(\rho\vec{U}\vec{U}\right) - \nabla \cdot \left(\mu\nabla\vec{U}\right) - \left(\nabla\vec{U}\right) \cdot \nabla\mu = -\nabla p_d - \vec{g} \cdot \vec{x}\nabla\rho + \sigma\kappa\nabla\gamma \quad [6]$$

where $\vec{U}$ (m s^{-1}) is the effective velocity vector shared by the two phases throughout the flow domain, which is defined as

$$\vec{U} = \gamma\vec{U}_l + (1-\gamma)\vec{U}_g \quad [7]$$

$\vec{U}_r = \vec{U}_l - \vec{U}_g$ is the relative velocity of liquid and gas at the interface, designated as "compression velocity", the subscript r here denotes "relative velocity"; γ, σ (N m^{-1}) and κ (m^{-1}) are the phase fraction, surface tension coefficient and mean curvature of the phase interface, respectively. p_d (Pa) is a modified pressure for simplifying the boundary conditions, defined as

$$p_d = p - \rho\vec{g} \cdot \vec{x} \quad [8]$$

where $\vec{x}$ (m) is the position vector and $\vec{g}$ (m s^{-2}) is the gravity vector, the subscript d denotes "dynamic". In this VOF model, the continuum surface force (CSF) model is adopted to account for the effects of surface tension at the liquid-gas interface by adding a force source f_σ (N) to Equation 5, which is defined as follow

$$f_\sigma = \sigma\kappa\nabla\gamma \quad [9]$$

the subscript σ denotes "surface tension", where the mean curvature of the phase interface κ is determined by:

$$\kappa = -\nabla \cdot \vec{n} = -\nabla \cdot \left(\frac{\nabla\gamma}{|\nabla\gamma|}\right) \quad [10]$$

It can be observed that κ is the interface curvature that is calculated with the divergence of the unit interface normal $\vec{n}$ and the unit interface normal $\vec{n}$ can be approximated with $\frac{\nabla\gamma}{|\nabla\gamma|}$. The surface unit normal $\vec{n}$ is adjusted in the cells adjacent to the wall according to the following equation:

$$\vec{n} = \vec{n}_w cos\theta + \vec{t}_w sin\theta \quad [11]$$

where $\vec{n}_w$ is the unit vector normal to the wall, $\vec{t}_w$ is the unit vector tangential to the wall, the subscript w denotes wall. θ (°) is the contact angle. In this study, only the constant contact angle is considered.

Oxygen diffusion model.—In a partially-saturated GDL, the local oxygen concentration C (mol m^{-3}) is governed by the diffusion equation:[39]

$$\nabla \cdot (D\nabla(C)) = 0 \quad [12]$$

where D (m^2 s^{-1}) is the oxygen diffusion coefficient. At the phase interface between air and liquid water, the concentration equilibrium is characterized by Henry law:

$$He = \frac{C_g}{C_l} \quad [13]$$

where He is constant Henry coefficient, and a value of 42.785 was chosen in this study.[38] To consider the oxygen transport in both air and water conveniently, a scalar C_e (mol m^{-3}) named as effective concentration is introduced:[39]

$$C_e = \begin{cases} C & \text{inside the gas phase} \\ CHe & \text{inside the liquid phase} \end{cases} \quad [14]$$

The final governing equation for C_e is written as:

$$\nabla \cdot (D_e \nabla C_e) = 0 \quad [15]$$

where D_e (m^2 s^{-1}) is the effective diffusion coefficient which written as:[40]

$$D_e = \left[\gamma\left(\frac{D_l}{He}\right)^{-1} + (1-\gamma)\left(\frac{D_g}{1}\right)^{-1}\right]^{-1} \quad [16]$$

where γ is the water phase fraction defined in previous VOF model, D_l (m^2 s^{-1}) and D_g (m^2 s^{-1}) are the oxygen diffusion coefficient in the liquid and gas phase, respectively. Here, the D_l and D_g are 1.97 $\times$ 10^{-9} m^2 s^{-1} and 2.19 $\times$ 10^{-5} m^2 s^{-1}, respectively.[27] Under dry condition, the water phase fraction γ is zero and all the diffusivity is set to D_g.

Stochastic model.—Toray carbon paper consists of numerous horizontally orientated straight fibers, as in Fig. 1 and Fig. 2a. The Toray carbon paper TGP-H-120 and TGP-H-060 are digitally reconstructed using a stochastic method,[17–20,27,29,37,41] as shown in Fig. 2b. For the dry GDL, the Toray-H-120 carbon paper with and without PTFE loadings are both considered. For partially-saturated GDLs, the Toray-H-120 carbon and Toray-H-060 without PTFE reconstruction are considered. Based on the GDL reconstruction method in our previous study,[37,41] the carbon paper without PTFE treatment is firstly reconstructed. After generating fiber structures of the GDL without PTFE (Toray-H-120 0 wt% PTFE), the PTFE is added by randomly filling the pore volume close to fibers. This process was repeated until the target PTFE loading was achieved.

Initial and boundary conditions.—*Two-phase VOF model.*—Two kinds of GDL samples (Toray-H-120 and Toray-H-060 carbon papers) with a cross-section of 400 μm $\times$ 400 μm are investigated this study. The water saturation distribution in a GDL was obtained by performing a water-invasion process where a constant pressure difference was imposed on the two sides of a GDL, as shown in Fig. 2c. This water-invasion process was used in previous studies to obtain local water saturation profiles in GDLs.[31,33,36] The side walls were assumed symmetric planes. The contact angle θ is set as 109° for carbon fiber.[37,41] Initially, there was no liquid water in GDLs.

Oxygen transport model.—To calculate the effective diffusivity of a partially-saturated GDL, oxygen diffusion was simulated based on the three-dimensional (3D) water field predicted from the above VOF model. For dry GDLs, the field γ is set zero, i.e. no water inside the GDL. The Dirichlet boundary condition for the effective oxygen concentration $\tilde{C}$ was imposed at the two opposite boundaries, while the others were considered as symmetry planes, as shown in Fig. 2d. The effective oxygen diffusivity D_{eff} (m^2 s^{-1}) was calculated as:

$$D_{eff} = \frac{J \cdot L}{A\Delta C_e} \quad [17]$$

where A (m^2) is the cross-sectional area of the GDL of the plane perpendicular to the diffusion direction (TP or IP direction). L (m) is the thickness of the GDL along the diffusion direction. ΔC_e (mol m^{-3}) is the effective concentration difference at the two opposite boundaries in the diffusion direction (assigned to be one and zero at the inlet and outlet boundary, respectively). J (mol s^{-1}) is the total oxygen flux at the outlet boundary. D_{eff} in the TP (y direction) and in the two IP (x and z direction) directions were calculated.

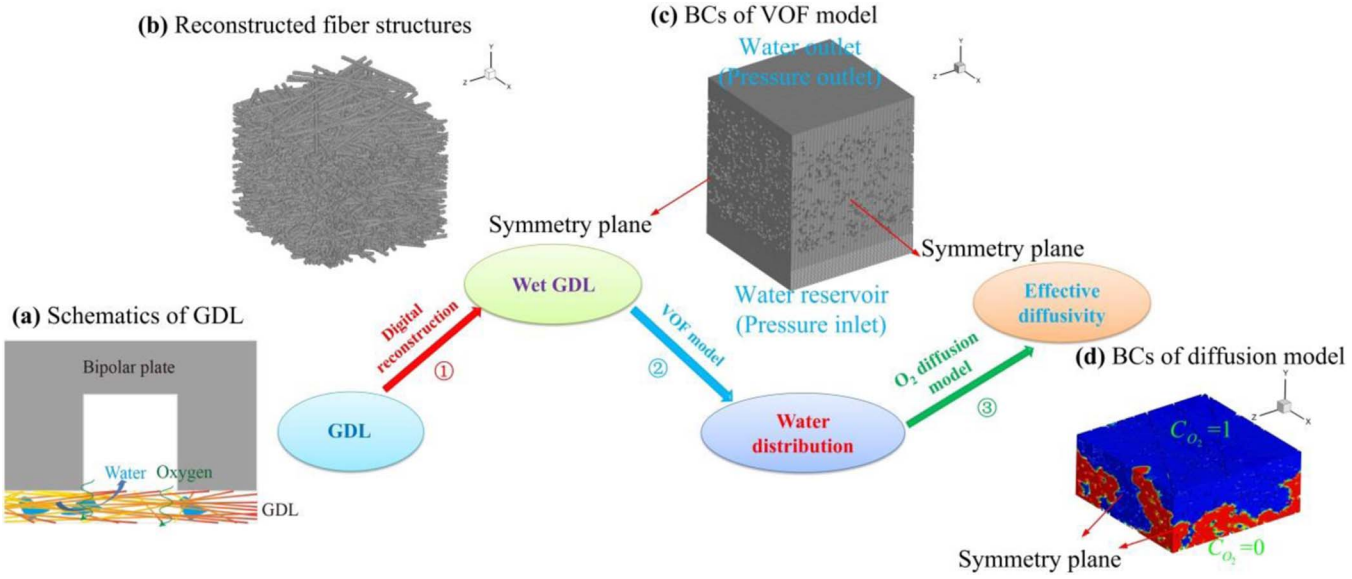

Figure 2. Model development of oxygen diffusion in the partially-saturated GDL. (a) Schematic of oxygen diffusion in the in- and through-plane directions of a partially-saturated GDL; (b) Reconstructed fiber structures; (c) and (d) Computational domains and boundary conditions of two-phase VOF model and the through-plane oxygen diffusion model, respectively.

Numerical procedures.—The computational domains of TGP-H-120 and TGP-H-060 carbon paper were discretized with about 4 million and 2 million of hexahedral mesh (160 × 148 × 160 and 160 × 96 × 160, x, y, z respectively), as shown in Fig. 2c. The open source software Open FOAM recently becomes popular in fuel cell modeling studies because of its strong support to custom specialized solvers[42-44] and was adopted in this study. The pressure-implicit with splitting of operators (PISO) and semi-implicit method for pressure linked equation (SIMPLE) schemes were employed to solve governing equations of two-phase VOF and oxygen diffusion models, respectively. The model parameters are summarized in Table II. The open-MPI was adopted for parallel computation. The time step was set 4×10^{-7} s for VOF model. Each two-phase VOF case took about 7 hours by using 56 Intel Xeon @2.93 GHz processors in parallel.

Results and Discussion

Dry GDLs.—Firstly, the present model is compared with the Nam and Kaviany's result[11] (M-3 in Table I). A fibrous medium similar to Ref. 11 was digitally reconstructed, where the oxygen diffusion model

Table II. Model parameters used in the model.

Model	Parameters	
	Numerical parameters	
Two-phase VOF	Algorithm	PISO
	Momentum Predictor	No
	nNonOrthogonalCorrectors	0
	nAlphaSubCycles	2
	Residual tolerance	1×10^{-8}
	Physical parameters	
	Dynamic viscosity ($m^2\ s^{-1}$)	Water: 1×10^{-6} Air: 1.48×10^{-5}
	Density ρ ($kg\ m^{-3}$)	Water: 1000 Air: 1
	Surface tension coefficient σ ($N\ m^{-1}$)	0.07
	Numerical parameters	
Oxygen diffusion	Algorithm	SIMPLE
	nNonOrthogonalCorrectors	0
	Relaxation factor	1
	Residual tolerance	1×10^{-8}
	Physical parameters	
	Diffusion coefficient D ($m^2\ s^{-1}$)	Water: 1.97×10^{-9} Air: 2.19×10^{-5}

Note: nNonOrthogonalCorrectors refers to the number of non-orthogonal correctors; nAlphaSubCycles refers to the number of sub-cycles when solving the γ equation. Sub-cycles are additional solutions to an equation within a given time step.

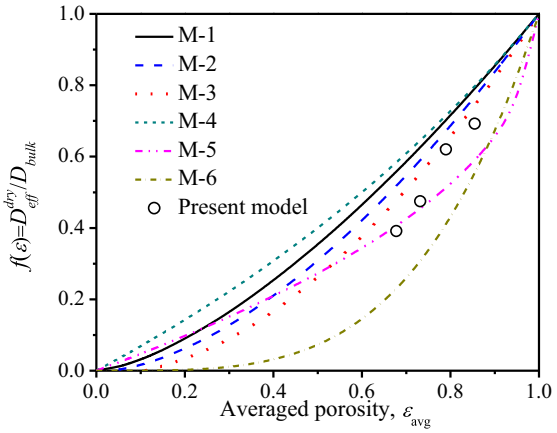

Figure 3. Relative effective oxygen diffusivity $f(\varepsilon)$ along the TP direction predicted by various models.

was applied. A sample of 396 μm × 400 μm × 396 μm was chosen for calculation. The relative effective oxygen diffusivity $f(\varepsilon)$ in the TP direction, predicted by the present model, is 0.476, which is close to the result of $f(\varepsilon) = 0.446$ in Ref. 11.

The present oxygen diffusion model was also compared with several diffusivity models (see Table I) that are based on several reconstructed GDLs of uniform porosity. It can be seen from Fig. 3 that the predicted $f(\varepsilon)$ in the TP direction is mostly close to the M-3 under large porosity and close to the M-5 under small porosity. It is noted that the M-3 and M-5 are close to each other under small porosity and a reasonable agreement between the present results and these two models was obtained. It can also be seen the predicted value always deviate the M-1, especially for small porosity. The M-1, i.e. the Bruggeman correlation, is originally developed for the electrical conductivity through spherical dielectric particles, which is different with the fibrous structures in GDLs.

To compare the present diffusion model with experimental data, the relative effective oxygen diffusivity $f(\varepsilon)$ along the TP direction in reconstructed GDL Toray-H-120 with different PTFE loadings were investigated and validated with experimental data from Zamel et al.[6] and Hwang et al.,[7] as shown in Fig. 4. The digital addition of PTFE loading was introduced in the Stochastic model section. It can be seen that the predicted value for the GDL without PTFE loading is higher than the experimental data. The predicted value is mostly close to the experimental data for 10 wt% PTFE loading and deviate experimental data again for high PTFE loading of 20 wt%. The reason for the

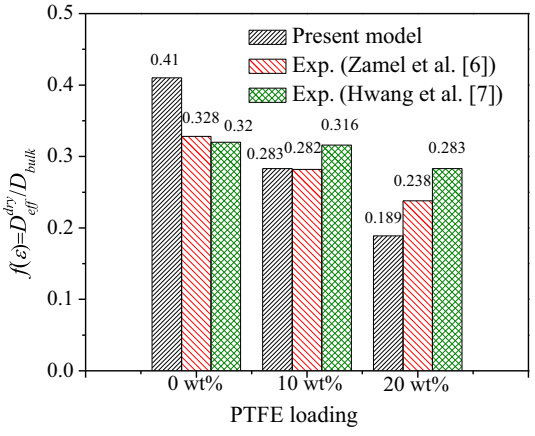

Figure 4. Comparison of predicted relative effective oxygen diffusivity $f(\varepsilon)$ along the TP direction with experimental data in dry GDLs of various PTFE loadings.[6,7]

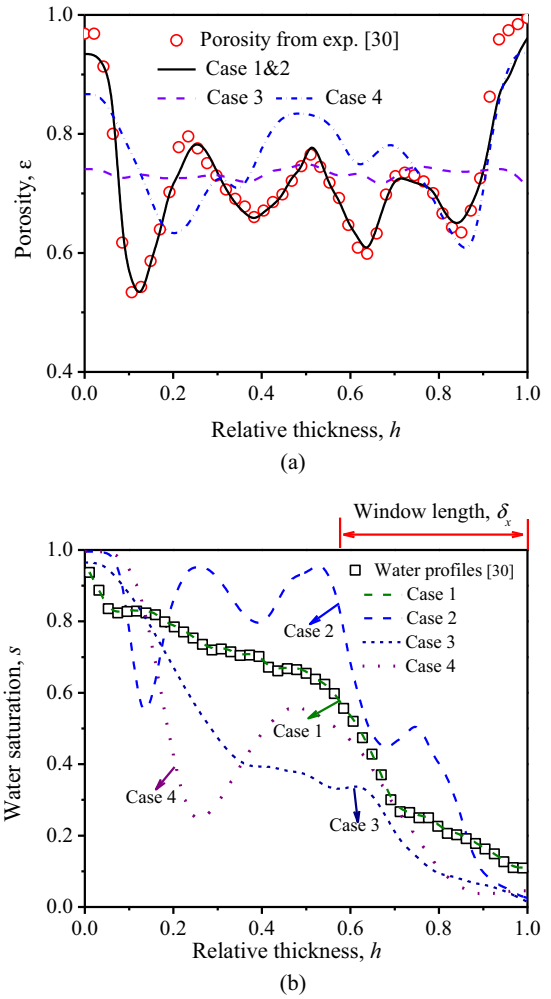

Figure 5. Local porosity and water saturation distributions in the TP direction for Cases 1–4. (a) Porosity ε; (b) Water saturation *s*.

deviation may be the difference in the local PTFE distribution between the reconstructed and experimental GDLs. The PTFE distribution in the TP direction of the real GDL can be significantly affected by different PTFE drying conditions,[41,45] the air drying method causes higher PTFE contents near the two sides of a GDL, thereby effectively hampering oxygen diffusion. In the present study, the PTFE loading is assumed to be randomly distributed in the GDL due to lack of the experimental data of the PTFE distribution.

Partially-saturated GDLs.—A total of four cases with different local porosity and water saturation were considered in this study. The detailed settings are listed in Table III. For Case 1, the local water saturation profile was obtained by randomly forming small droplets (droplet diameter is about 40 um) inside the GDL until the final water saturation profile along the TP direction reaches the profile in Ref. 31, as shown in Fig. 5b (green line and black box). The relative thickness h is defined as the dimensionless thickness (i.e. $h = 0$ at the GDL bottom and $h = 1$ at the GDL top). The reproduction of this water profile is intended to validate the predicted relative effective oxygen effective diffusivity in partially-saturated GDL $g(s)$ with LB data from Ref. 31. For Case 2, the local water saturation profile was obtained by performing water-invasion in the reconstructed GDL Toray-H-120 using the VOF model. It is noted that the reconstructed GDLs in both Case 1 and Case 2 are same and the local porosity distribution is shown in Fig. 5a. For Case 3, a thin GDL (192 μm) with uniform porosity was considered to investigate the effect of different local porosity distribution on the effective oxygen diffusivity $g(s)$. The water

Table III. Operating conditions of Cases 1–4.

Case	GDL	Thickness (μm)	Porosity	Pressure difference (kPa)	Window length δ_x (μm)
1	Toray-H-120	376	Ref. 31	4	16, 56, 110, 164, 218, 262
2	Toray-H-120	376	Ref. 31	10	16, 56, 110, 164, 218, 262
3	Customize	192	Uniform (0.73)	6	24, 48, 72, 96, 120, 144, 168
4	Toray-H-060	192	Ref. 37	6	19.4, 36.8, 62.9, 89, 115.1, 141.2, 167.3

saturation profile of Case 3 is also obtained by performing water-invasion in the reconstructed GDL using the VOF model. The water saturation profile along the TP was shown in Fig. 5b. For Case 4, a sample of Toray-H-060, reconstructed in our previous paper,[37] was considered. The local water saturation profile of this GDL was also form the previous VOF model,[37] as shown in Fig. 5b.

Different wet GDL samples were obtained by cutting partially-saturated GDLs with different window length δ_x (μm), as shown in Fig. 5b. The computed relative effective oxygen diffusivity $g(s)$ along the TP direction of four cases are summarized in Fig. 6a. It can be seen that the predicted $g(s)$ in Case 1 agrees reasonably with the LB model.[31] The correlation of $g(s)$ and water saturation follows the power law $g(s) = (1\text{-}s)^{\lambda}$, and the exponent λ is found close to 2, which is smaller than the value ($\lambda = 3$ for the TP direction) proposed by Nam and Kaviany.[11] The reason may be the assumption of the random distribution of droplets inside the GDL in Case 1. For Case 2, it can be seen that $g(s)$ is close to the power law curve of $g(s) = (1\text{-}s)^3$ under

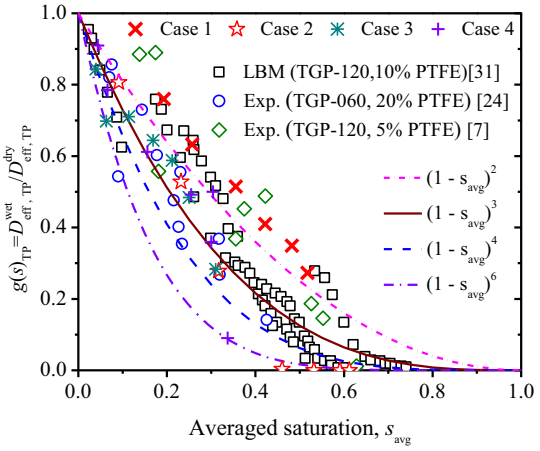

(a) Through plane (TP)

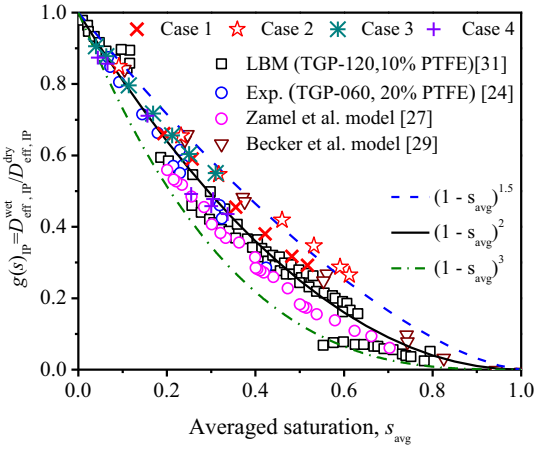

(b) In-plane (IP)

Figure 6. Comparison of predicted relative effective oxygen diffusivity $g(s)$ with LB model results,[31] PM model results[27,29] and experimental data.[7,24] (a) TP direction; (b) IP direction.

the small water saturation range, but deviates the curve under large water saturation (about s = 0.5∼0.6). For Case 3, the predicted $g(s)$ agrees well with the experimental data[24] and power law curve $g(s) = (1\text{-}s)^3$. For Case 4, the predicted $g(s)$ agrees reasonably with the experimental data[24] and power law curve $g(s) = (1\text{-}s)^3$, except several points deviate. This is because a water saturation bump appears in the middle region of the GDL, as shown in Fig. 5b, which effectively blocks oxygen diffusion despite that the averaged saturation is still small in the GDL sample. In summary, both the local water saturation profile and porosity distribution have significant effects on the relative oxygen effective diffusivity $g(s)$.

The computed relative effective oxygen diffusivity $g(s)$ along the IP direction of the four cases are summarized in Fig. 6b. The averaged value of two IP directions is computed for comparison. It can be seen that the predicted $g(s)$ agrees well with data from the LB model[31] and power law curve $g(s) = (1\text{-}s)^2$ proposed by Nam and Kaviany[11] under the small water saturation, but deviates under large water saturation. The reason is same as that in the TP direction. For Case 2–4, the predicted $g(s)$ agrees well with the LB model[31] and experimental data.[24] The PM model from Zamel et al.[27] and Becker et al.[29] for the partially-saturated GDL were also plotted for comparison. For Case 1–3, the predicted $g(s)$ is closer to the model of Becker et al.,[29] while for Case 4, the predicted $g(s)$ is closer to Zamel et al.[27] In general, the predicted $g(s)$ in the four cases agree well with various experimental data and models, and the different local water saturation and porosity distributions have minor effects on $g(s)$ in the IP direction than the TP one.

Local oxygen concentration in dry and partially-saturated GDLs.—Fig. 7 shows the 3D liquid water and oxygen concentration distributions in both dry and partially-saturated GDL samples of Case 3 (window length $\delta_x = 168$ μm). The oxygen diffusion in both TP and two IP directions are considered. It can be observed that the oxygen diffusion in the GDL is significantly affected by the presence of liquid water in both TP and IP directions. The TP oxygen diffusion is more sensitive to the presence of liquid water. Fig. 8 shows the averaged oxygen concentration C_{O_2} (mol m^{-3}) distribution in both TP and IP (x) directions. It can be seen that the C_{O_2} distribution in the TP direction of the partially-saturated GDL is much higher than that in the dry GDL while minor difference is presented for the IP direction. This is because the very high water saturation near the GDL bottom, where water is injected, severely hampers oxygen diffusion in the TP direction.

Conclusions

In this study, oxygen diffusion in both dry and partially-saturated gas diffusion layer (GDL) was investigated by an oxygen diffusion model, in conjunction with a two-phase volume of fluid (VOF) model. A stochastic method was adopted to reconstruct the microstructures of various GDLs. Four partially-saturated GDLs of different local porosity and water saturation distributions were investigated. The relative oxygen diffusivity in the through-plane (TP) and in-plane (IP) directions were predicted and compared with other works, including the lattice Boltzmann (LB) models, pore-morphology (PM) model and experimental data.

1. An oxygen diffusion model was developed to describe oxygen diffusion in both dry and partially-saturated GDLs. A two-phase VOF model in our previous work was adopted to obtain the

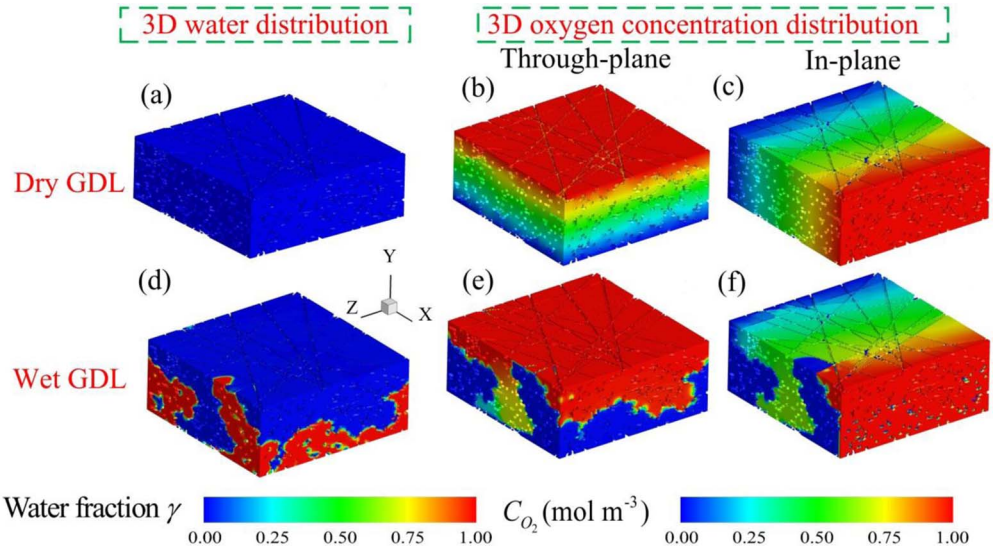

Figure 7. Computed 3D liquid water distributions and oxygen concentration fields in both dry and partially-saturated GDL samples of Case 3 (the window length $\delta_x = 168$ μm). (a) and (d) 3D water distribution in dry and partially-saturated GDL; (b) and (c): Oxygen concentration field in the dry GDL; (e) and (f) Oxygen concentration field in the partially-saturated GDL.

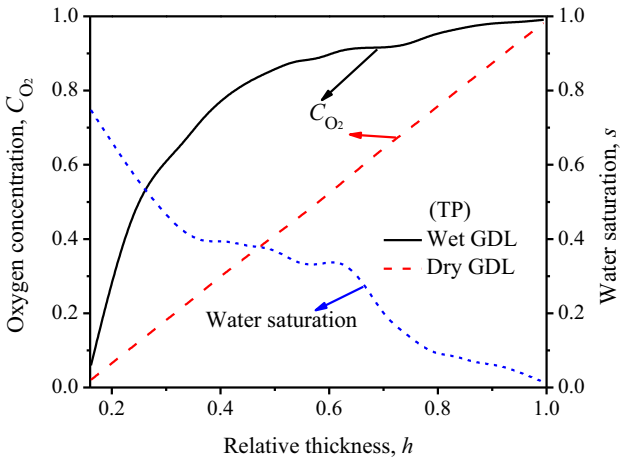

(a) Through plane (TP)

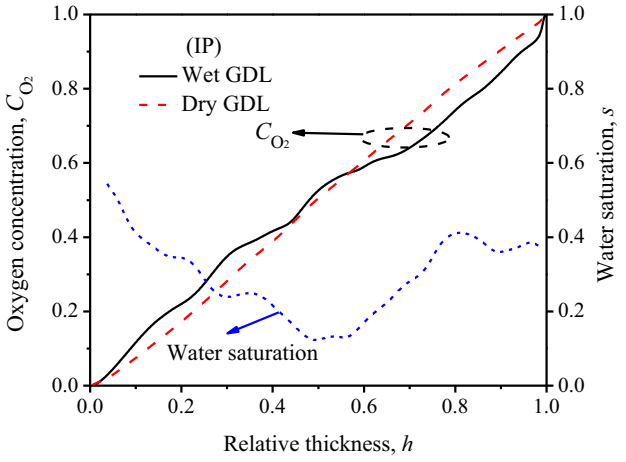

(b) In-plane (IP)

Figure 8. Local averaged water saturation s and oxygen concentration C_{O_2} distribution along the TP and IP directions in the GDL sample of Case 3 (the window length $\delta_x = 168$ μm). (a) TP direction; (b) IP direction.

three-dimensional (3D) liquid water distribution in reconstructed GDLs.

2. The relative effective oxygen diffusivity in the dry GDL, $f(\varepsilon)$, was validated with various models. The predicted $f(\varepsilon)$ agreed reasonably well with Nam and Kaviany (2003).
3. The $f(\varepsilon)$ in the dry TGP-H-120 of various PTFE loadings was investigated and compared with experimental data. A good agreement was achieved for the PTFE loading of 10%. There was about 20–30% difference for the other two PTFE loadings.
4. For the four partially-saturated GDLs, the predicted $g(s)$ generally followed the power law $g(s) = (1\text{-}s)^{\lambda}$ ($\lambda = 3$ for the TP direction and 2 for the IP). Good agreement with experimental data was obtained for several cases.
5. The $g(s)$ in the TP direction is more sensitive to the presence of liquid water than the IP one, and local water saturation and porosity distributions have much more significant effects on the $g(s)$ in the TP direction.

The present two-phase VOF model in conjunction with the oxygen diffusion model can be further extended to other types of GDLs, such as Freudenberg and SGL carbon papers, by using their corresponding microstructures.

Acknowledgments

This work is supported by the National Natural Science Foundation of China for Excellent Young Scholars (grant No. 51622606), and the Key Program of Natural Science Foundation of Tianjin (China) (grant No. 16JCZDJC30800). Y. Wang also thanks Shanghai Everpower Technologies Ltd for partial financial support. The first author also thanks PhD student Jinhua Lu for insightful discussion.

ORCID

Zhiqiang Niu https://orcid.org/0000-0001-9220-282X
Yun Wang https://orcid.org/0000-0003-2035-3148

References

1. Y. Wang, K. S. Chen, J. Mishler, S. C. Cho, and X. C. Adroher, *Applied energy*, **88**, 981 (2011).
2. J. H. Nam, K.-J. Lee, G.-S. Hwang, C.-J. Kim, and M. Kaviany, *International Journal of Heat and Mass Transfer*, **52**, 2779 (2009).
3. M. Mathias, J. Roth, J. Fleming, and W. Lehnert, *Handbook of fuel cells*, (2003).

4. Y. Wang and K. S. Chen, *PEM fuel cells: thermal and water management fundamentals*, Momentum Press (2013).
5. Y. Wang, *Journal of Power Sources*, **185**, 261 (2008).
6. N. Zamel, N. G. Astrath, X. Li, J. Shen, J. Zhou, F. B. Astrath, H. Wang, and Z.-S. Liu, *Chemical Engineering Science*, **65**, 931 (2010).
7. G. Hwang and A. Weber, *Journal of The Electrochemical Society*, **159**, F683 (2012).
8. R. Flückiger, S. A. Freunberger, D. Kramer, A. Wokaun, G. G. Scherer, and F. N. Büchi, *Electrochimica Acta*, **54**, 551 (2008).
9. D. Bruggeman, *Annals of Physics*, **416**, 636 (1935).
10. M. M. Tomadakis and S. V. Sotirchos, *AIChE Journal*, **39**, 397 (1993).
11. J. H. Nam and M. Kaviany, *International Journal of Heat and Mass Transfer*, **46**, 4595 (2003).
12. P. K. Das, X. Li, and Z.-S. Liu, *International Journal of Hydrogen Energy*, **35**, 2403 (2010).
13. M. M. Mezedur, M. Kaviany, and W. Moore, *AIChE journal*, **48**, 15 (2002).
14. M. J. Martínez, S. Shimpalee, and J. Van Zee, *Journal of The Electrochemical Society*, **156**, B80 (2009).
15. N. Zamel and X. Li, *Progress in energy and combustion science*, **39**, 111 (2013).
16. J. Becker, R. Flückiger, M. Reum, F. N. Büchi, F. Marone, and M. Stampanoni, *Journal of The Electrochemical Society*, **156**, B1175 (2009).
17. Y. Wang, S. Cho, R. Thiedmann, V. Schmidt, W. Lehnert, and X. Feng, *International journal of heat and mass transfer*, **53**, 1128 (2010).
18. M. Espinoza-Andaluz, M. Andersson, and B. Sundén, *International Journal of Hydrogen Energy*, **42**, 11689 (2017).
19. Z. Niu, K. Jiao, Y. Wang, Q. Du, and Y. Yin, *International Journal of Energy Research*, (2018).
20. H. Ostadi, P. Rama, Y. Liu, R. Chen, X. Zhang, and K. Jiang, *Journal of Membrane Science*, **351**, 69 (2010).
21. J. P. Owejan, T. A. Trabold, and M. M. Mench, *International Journal of Heat and Mass Transfer*, **71**, 585 (2014).
22. Y. Utaka, I. Hirose, and Y. Tasaki, *International Journal of Hydrogen Energy*, **36**, 9128 (2011).
23. R. Koresawa and Y. Utaka, *International Journal of Heat and Mass Transfer*, **76**, 549 (2014).
24. T. Rosén, J. Eller, J. Kang, N. I. Prasianakis, J. Mantzaras, and F. N. Büchi, *Journal of The Electrochemical Society*, **159**, F536 (2012).
25. T. G. Tranter, P. Stogornyuk, J. T. Gostick, A. Burns, and W. F. Gale, *International Journal of Heat and Mass Transfer*, **110**, 132 (2017).
26. S. Wang and Y. Wang, *International Journal of Heat and Mass Transfer*, **98**, 541 (2016).
27. N. Zamel, X. Li, J. Becker, and A. Wiegmann, *International Journal of Hydrogen Energy*, **36**, 5466 (2011).
28. M. Bosomoiu, G. Tsotridis, and T. Bednarek, *Journal of Power Sources*, **285**, 568 (2015).
29. J. Becker, V. Schulz, and A. Wiegmann, *Journal of fuel cell science and technology*, **5**, 021006 (2008).
30. D. Zhang, Q. Cai, and S. Gu, *Electrochimica Acta*, (2018).
31. P. A. García-Salaberri, G. Hwang, M. Vera, A. Z. Weber, and J. T. Gostick, *International Journal of Heat and Mass Transfer*, **86**, 319 (2015).
32. T. Bednarek and G. Tsotridis, *Journal of Power Sources*, **340**, 111 (2017).
33. P. A. García-Salaberri, J. T. Gostick, G. Hwang, A. Z. Weber, and M. Vera, *Journal of Power Sources*, **296**, 440 (2015).
34. R. Wu, Q. Liao, X. Zhu, and H. Wang, *International Journal of Heat and Mass Transfer*, **54**, 4341 (2011).
35. R. Wu, X. Zhu, Q. Liao, H. Wang, Y.-D. Ding, J. Li, and D.-D. Ye, *Electrochimica Acta*, **55**, 7394 (2010).
36. S. M. Moosavi, M. Niffeler, J. Gostick, and S. Haussener, *Chemical Engineering Science*, **176**, 503 (2018).
37. Z. Niu, Y. Wang, K. Jiao, and J. Wu, *Journal of The Electrochemical Society*, **165**, F613 (2018).
38. H. Fathi, A. Raoof, S. Mansouri, and M. T. van Genuchten, *Journal of The Electrochemical Society*, **164**, F298 (2017).
39. D. Bothe, M. Koebe, K. Wielage, and H.-J. Warnecke, in *ASME/JSME 2003 4th Joint Fluids Summer Engineering Conference*, p. 423 (2003).
40. M. A. J. Nieves-Remacha, L. Yang, and K. F. Jensen, *Industrial & Engineering Chemistry Research*, **54**, 6649 (2015).
41. Z. Niu, Z. Bao, J. Wu, Y. Wang, and K. Jiao, *Applied Energy*, 2018 (under review).
42. M. Hafttananian, A. Ramiar, B. Shabani, and A. Ranjbar, *Electrochemica Acta*, **246**, 348 (2017).
43. S. Beale, H. Choi, J. Pharoah, H. Roth, H. Jasak, and D. Jeon, *Computer Physics Communications*, **200**, 15 (2016).
44. M. Hafttananian, A. Ramiar, and A. Ranjbar, *Energy Conversion and Management*, **122**, 564 (2016).
45. H. Ito, K. Abe, M. Nakano, T. Maeda, T. Munakata, H. Nakajima, and T. Kitahara, *J Power Sources*, **248**, 822 (2014).